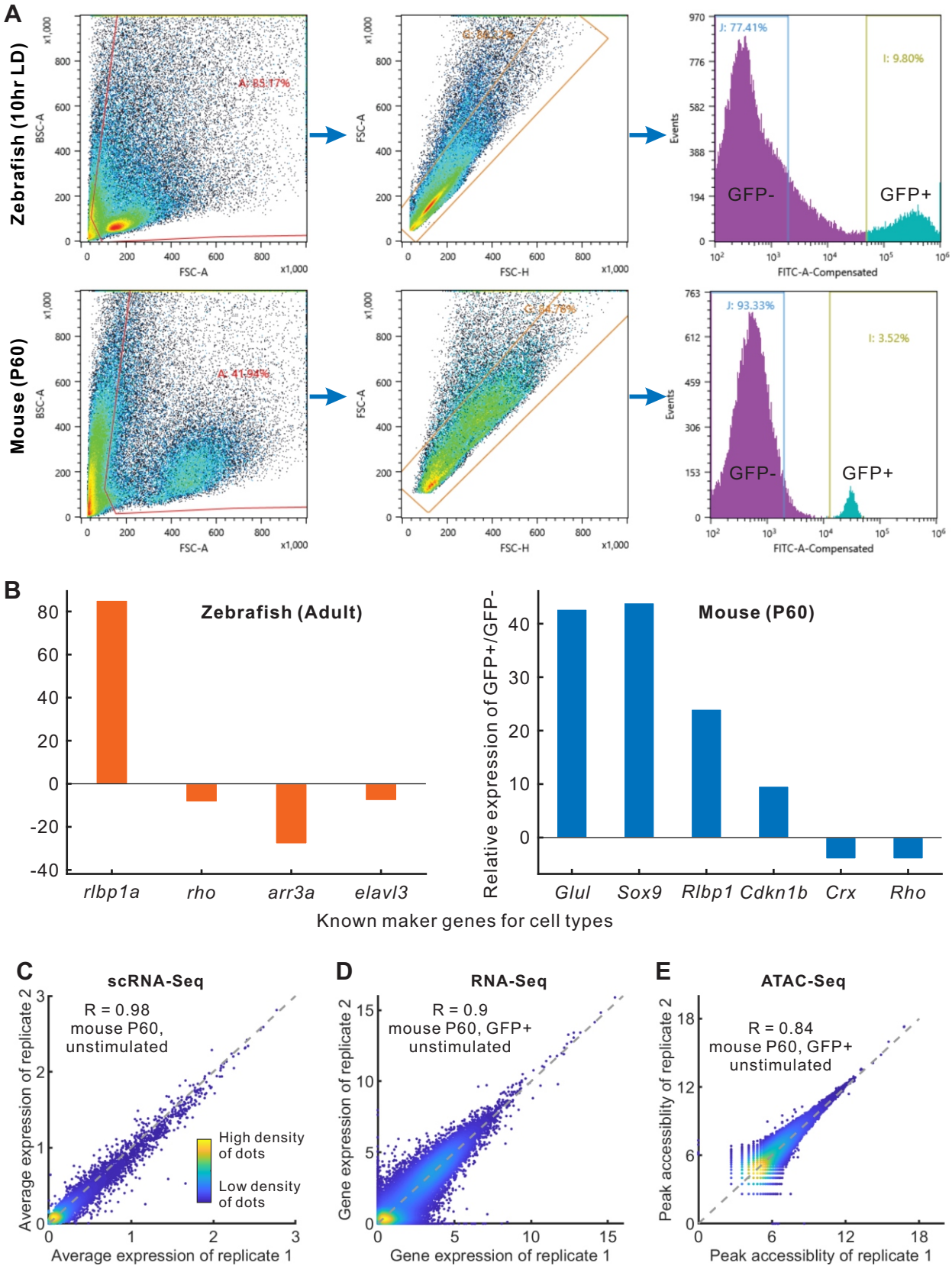

Figure S1, Hoang et al. Quality of measured samples and data. (A) Fluorescence activated cell sorting (FACS) strategy for isolation of GFP+ (MG) and GFP- (non-MG) samples. (B) Marker gene expression measured by RT-qPCR from FACS in adult zebrafish and Glast-Sun1/GFP P60 mice. (C-E) Correlation of two replicates from mouse P60 measured by scRNA-Seq, RNA-Seq and ATAC-Seq.

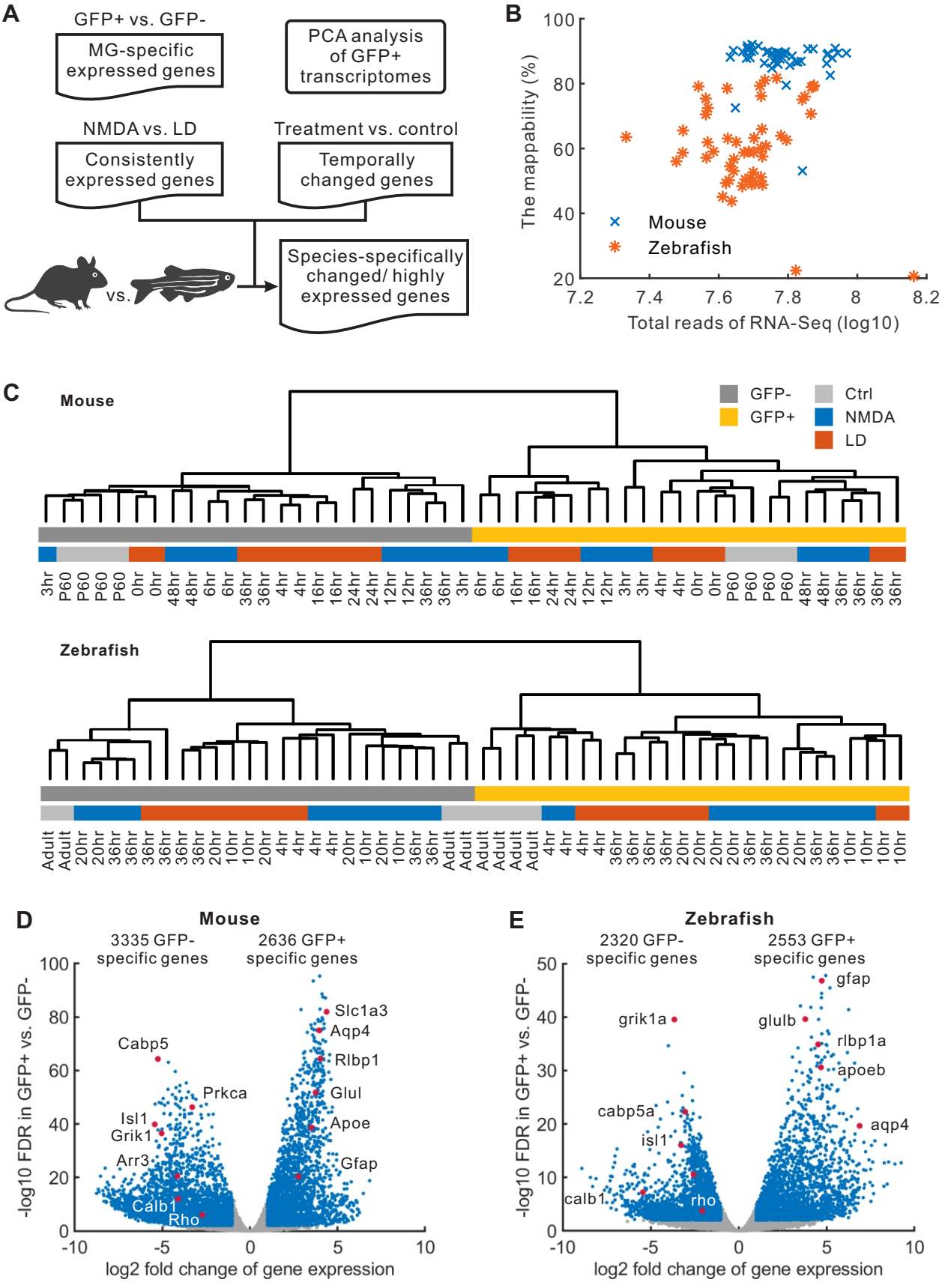

Figure S2, Hoang et al. Comparison of GFP+ and GFP- samples. (A) Analysis flow of RNA-Seq data. After identifying MG-specific expressed genes, we performed PCA (principal component analysis), and identified correlated and differentially expressed genes (DEGs) across multiple time points of NMDA and light damage (LD) models in mouse and zebrafish. (B) Quality of RNA-Seq data. (C) Hierarchical clustering of GFP+ and GFP- samples based on expression profiles of all genes. (D-E) Volcano plot of DEGs between GFP+ and GFP- samples. Blue dots are significantly DEGs (fold change > 2 and FDR < 0.01).

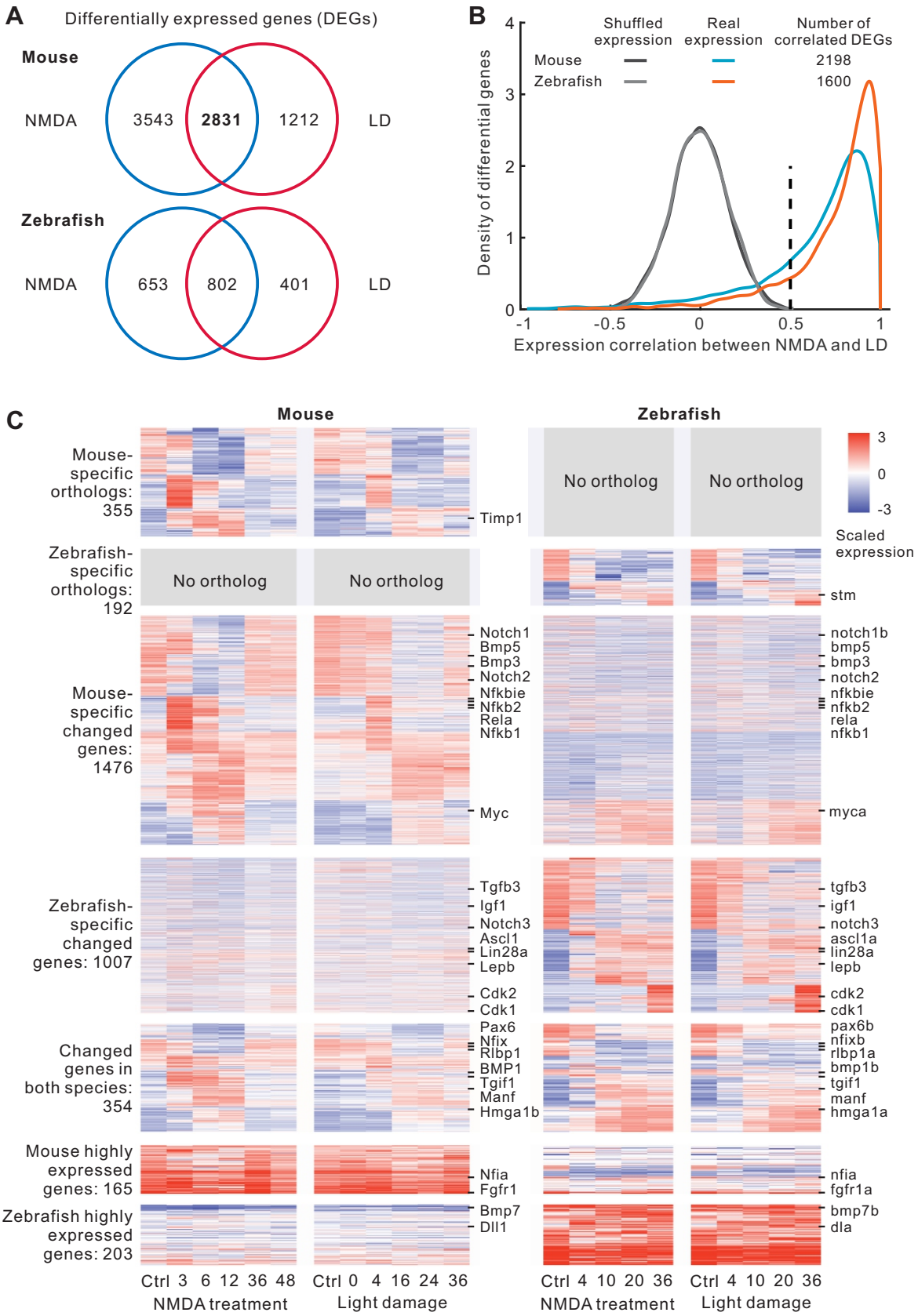

Figure S3, Hoang et al. Identification of differentially expressed genes (DEGs) in mouse and zebrafish MG. (A) Venn diagram of the number of significantly DEGs measured by RNA-Seq in NMDA and light damage (LD) models of mouse/zebrafish (fold change > 1.5 and FDR < 0.05). (B) Correlation of DEGs between two models. Shared DEGs in the mouse and all DEGs in the zebrafish were used to identify correlated DEGs (correlation > 0.5). (C) Heatmap of four broad categories of changed or highly expressed genes in each species. Scaled expression of GFP+ samples is shown for changed genes in each species, whereas relative expression of GFP+ to corresponding GFP- is shown for highly expressed genes in each species.

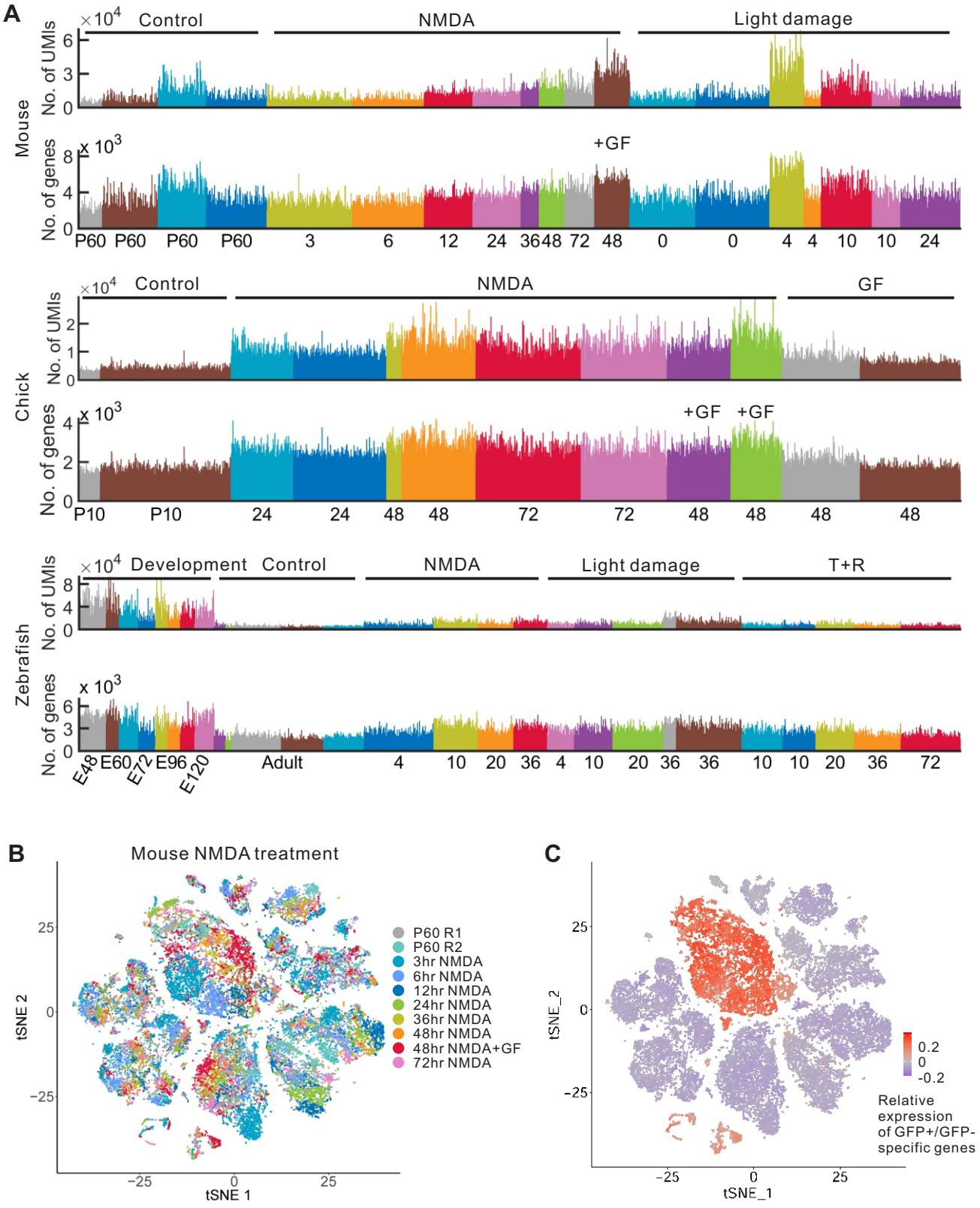

Figure S4, Hoang et al. Quality of single-cell RNA-Seq data. (A) Number of genes and UMIs in single cells. Each bar represents one cell. GF, growth factor (insulin+FGF). T+R, TNFα and RO4929097 treatment. (B) Clustering of retinal cells from mouse NMDA treatment. Cells are colored by samples. (C) Identification of MG using GFP+/GFP- specific expressed genes from bulk RNA-Seq analysis.

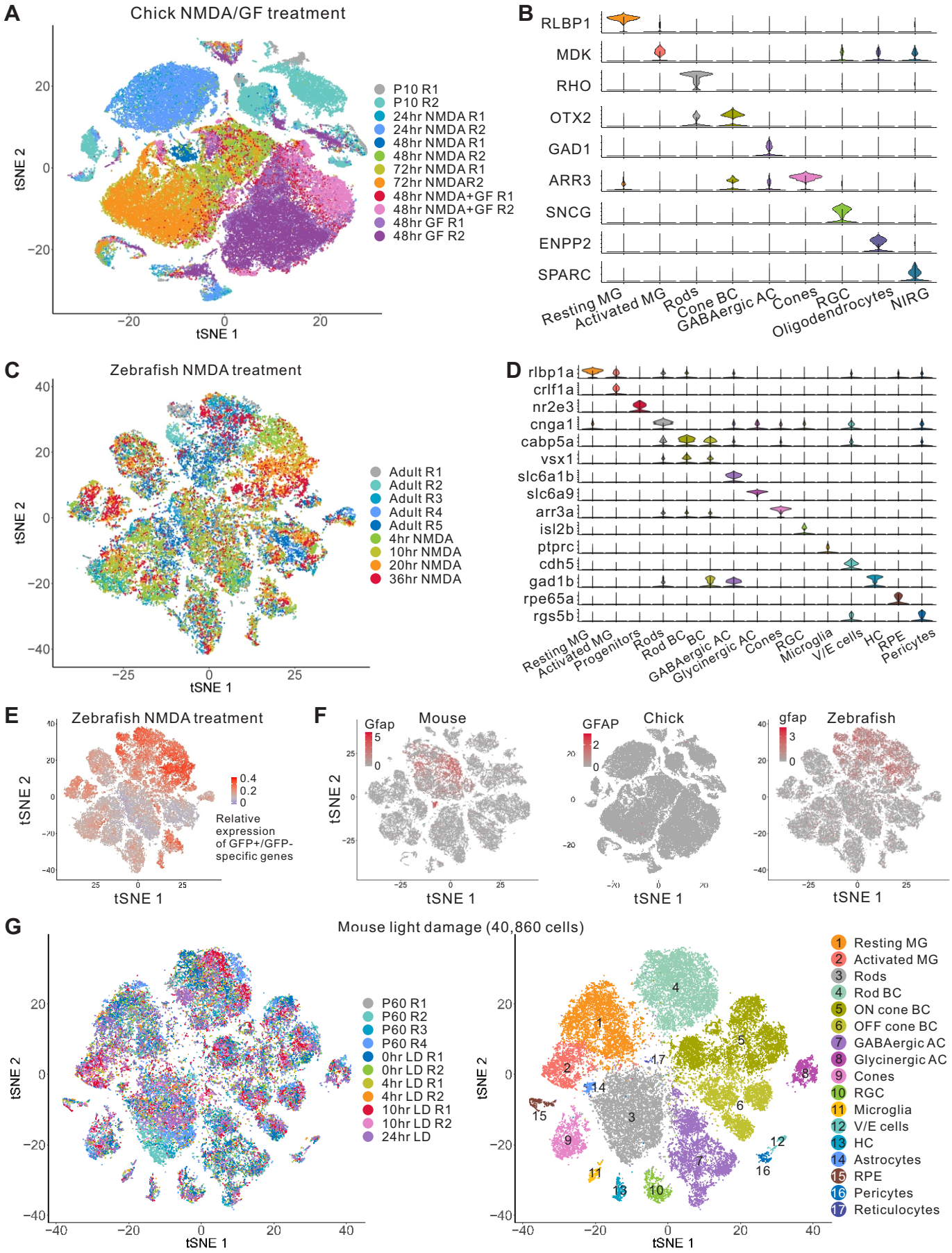

Figure S5, Hoang et al. tSNE view of whole retina cells. (A) Clustering of chick retinal cells colored by samples. (B) Expression of cell-type-specific markers in the chick. (C) tSNE view of retinal cells from zebrafish NMDA treatment samples. (D) Expression of cell-type-specific markers in zebrafish NMDA treatment samples. (E) Identification of zebrafish MG using GFP+/GFP- specific expressed genes from bulk RNA-Seq. (F) Single-cell expression of Gfap/GFAP/gfap in mouse, chick and zebrafish NMDA treatment. (G) tSNE view of retinal cells from mouse light damage samples.

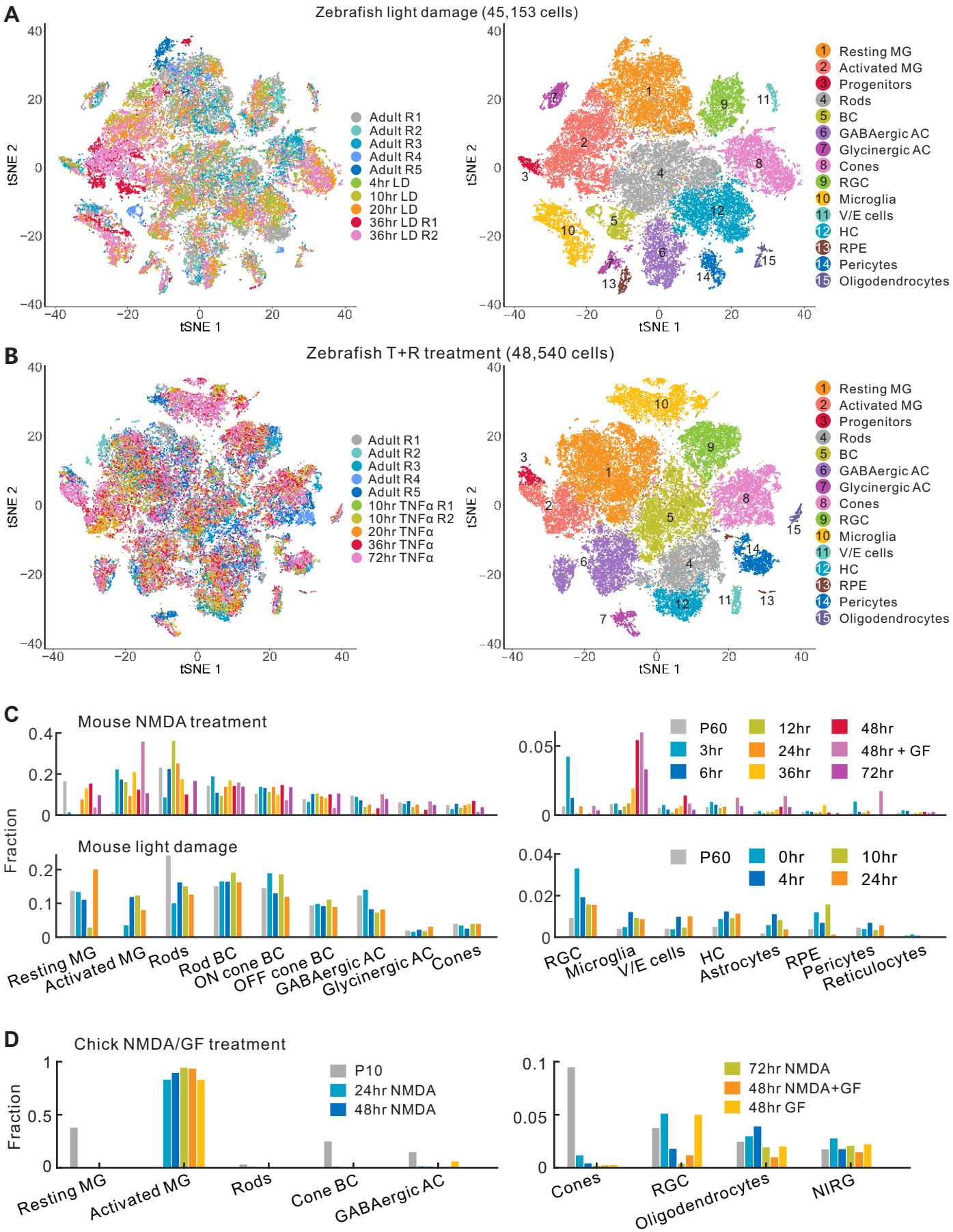

Figure S6, Hoang et al. Clustering of zebrafish retinal cells from light damage and TNFa+RO4929097 (T+R) treatment. (A) tSNE-view of retinal cells from zebrafish light damage. (B) tSNE-view of retinal cells from zebrafish T+R treatment. (C) Changes in mouse cell types following NMDA treatment and light damage. (D) Changes in chick cell types following NMDA/growth factor (GF) treatment.

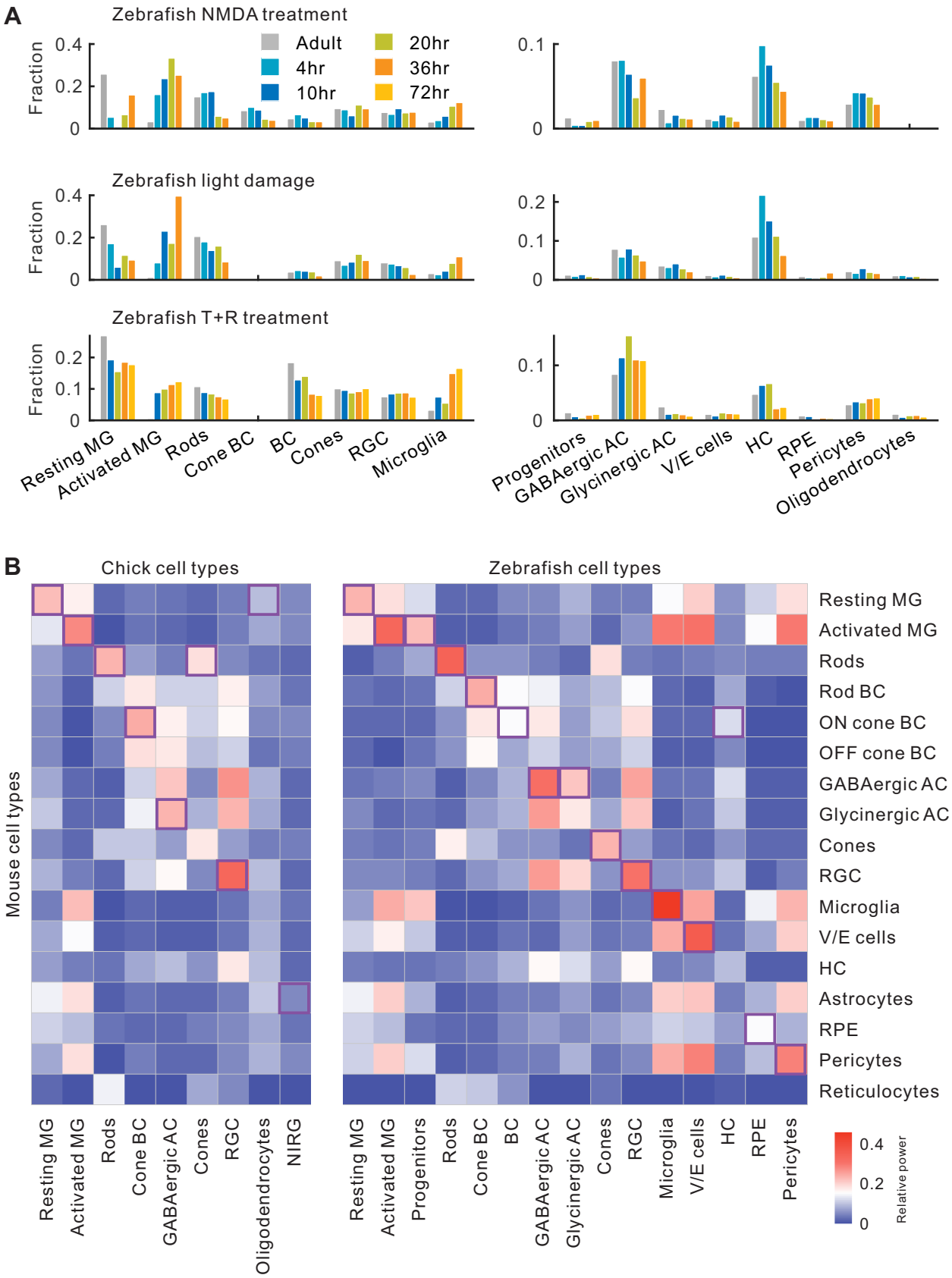

Figure S7, Hoang et al. Comparison of retinal cell types in species. (A) Changes in the fraction of zebrafish cell types following retinal injury. T+R, TNFa+RO4929097 treatment. (B) Comparison of cell types between chick/zebrafish and mouse. For each chick and zebrafish cell type, the most similar mouse cell types are highlighted in the purple box.

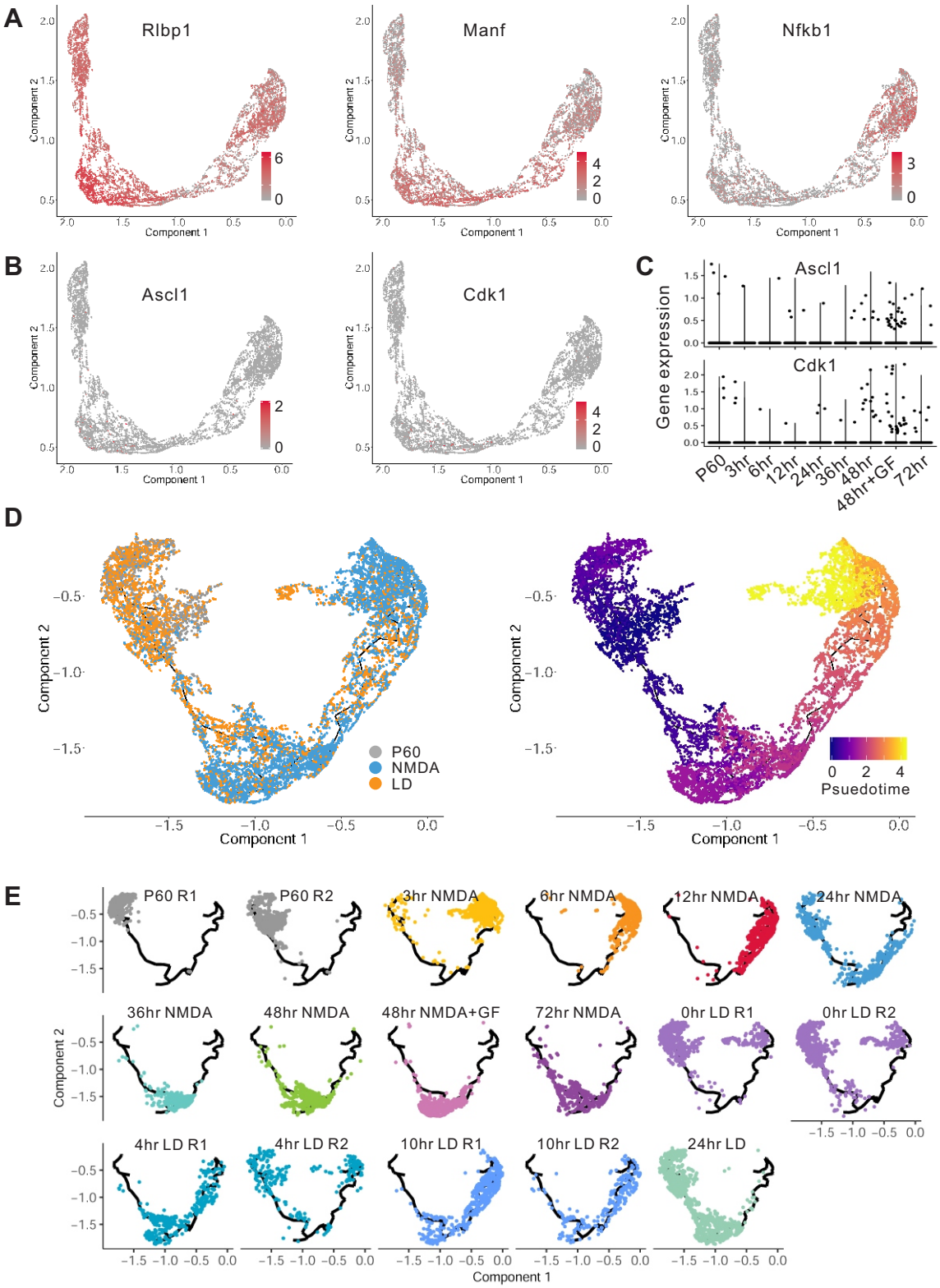

Figure S8, Hoang et al. Trajectory and features of mouse MG. (A-B) Expression of marker genes in mouse MG trajectory following NMDA treatment. (C) Expression of Ascl1 and Cdk1 at real time points of MG cells following NMDA treatment. GF, growth factor (insulin+FGF). (D-E) Trajectory of mouse MG following NMDA treatment and light damage (LD).

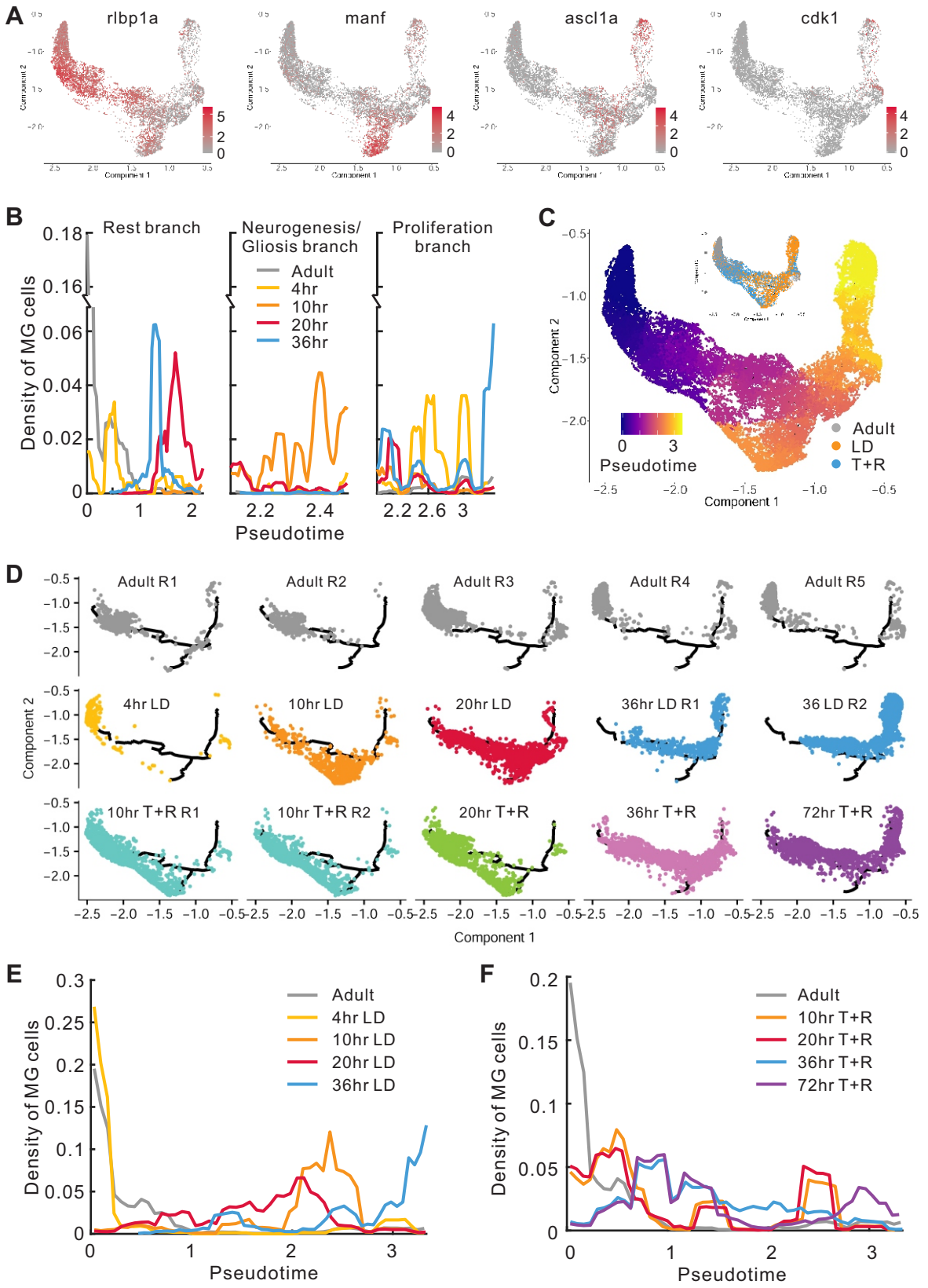

Figure S9, Hoang et al. Trajectory and features of zebrafish MG. (A) Gene expression of MG following NMDA treatment. (B)The density of zebrafish MG across pseudotime. (C-D) Trajectory of zebrafish MG from light damage (LD) and TNFa+RO4929097 (T+R) treatment. (E-F) The density of zebrafish MG across pseudotime following light damage and T+R treatment.

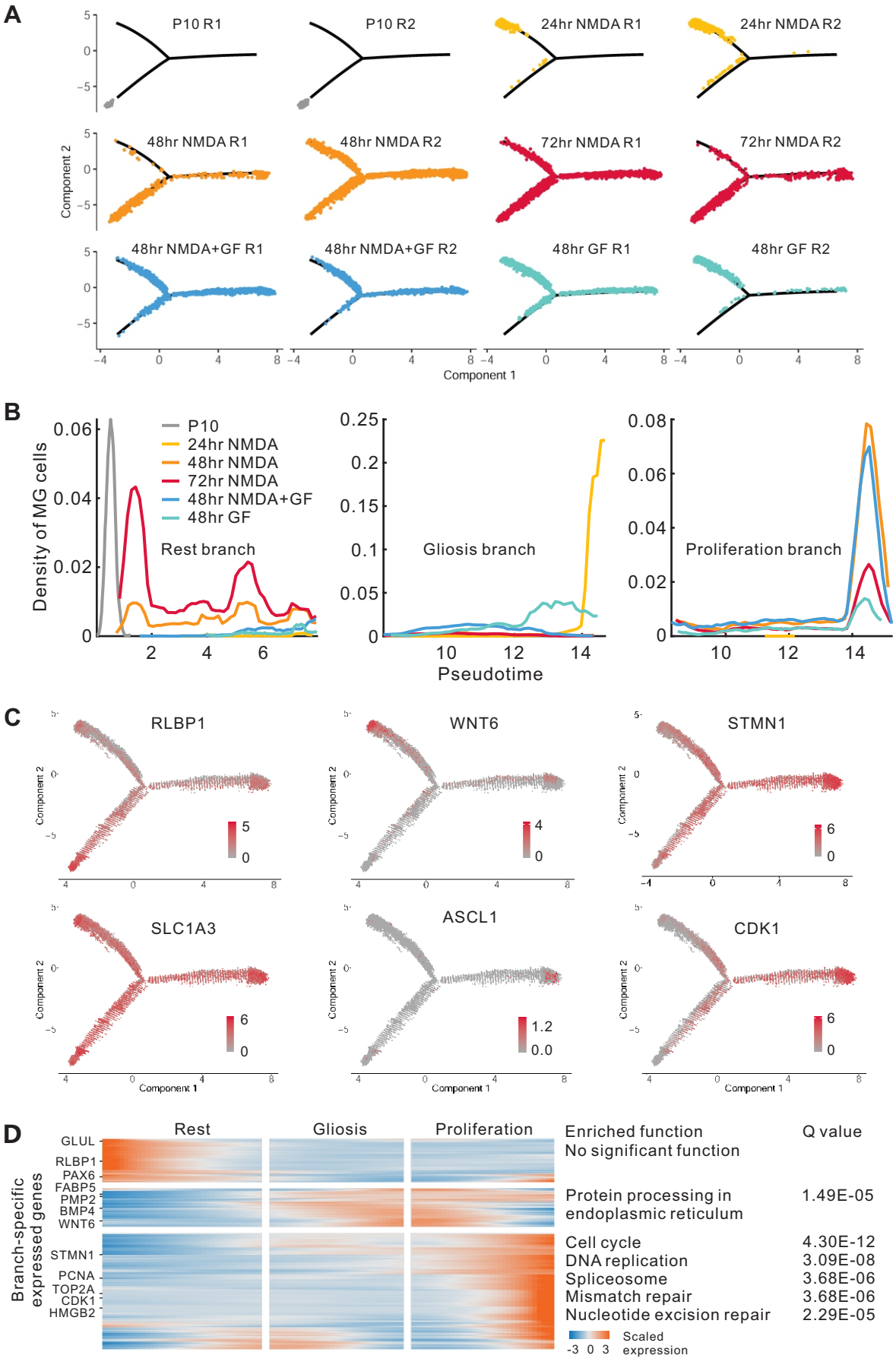

Figure S10, Hoang et al. Trajectory and features of chick MG. (A) Trajectory of chick MG separated by samples. GF, growth factor (insulin+FGF) treatment. (B) The density of MG across pseudotime. (C) Gene expression of MG in three branches. (D) Heatmap and enriched functions of branch-specific expressed genes in the chick.

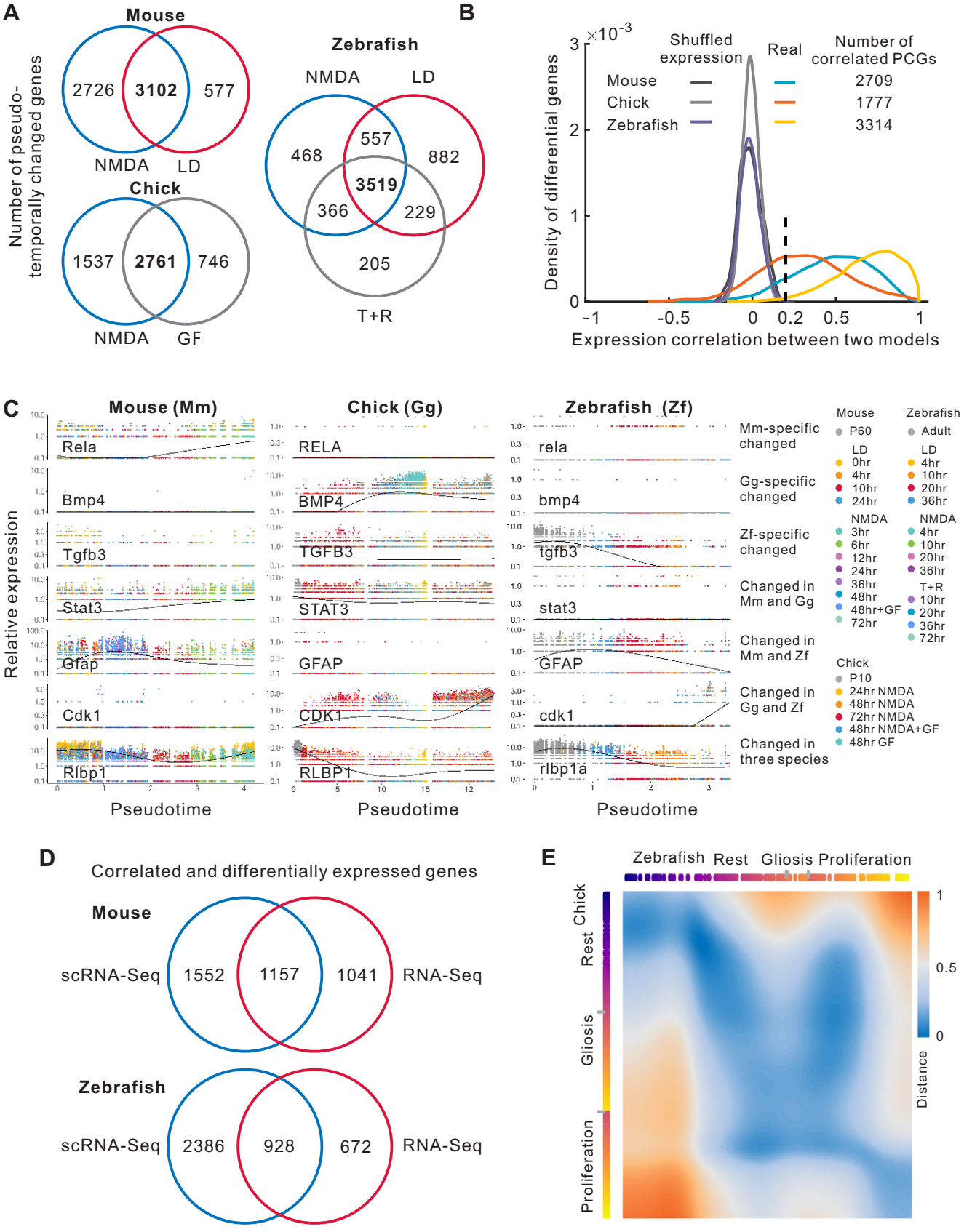

Figure S11, Hoang et al. Comparison of pseudo-temporally changed genes (PCGs) from mouse, chick and zebrafish MG. (A) Venn diagram of the number of PCGs from retinal damage/treatment models in three species (fraction of expressed cells > 0.01, single-cell expression difference > 0.1 and q-value < 0.001). LD, light damage. T+R, TNFa+RO4929097 treatment. GF, growth factor (insulin+FGF). (B) Distribution of PCG correlation between the two damage models. Correlated PCGs (cPCGs) are refined from PCGs shared by all models of each species. (C) Examples of species-specific or shared cPCGs. (D) Comparison of differentially expressed MG genes identified by analyzing scRNA-Seq and RNA-Seq data. (E) Alignment of two MG trajectories from chick and zebrafish. The trajectory with branch information was colored to indicate pseudotime.

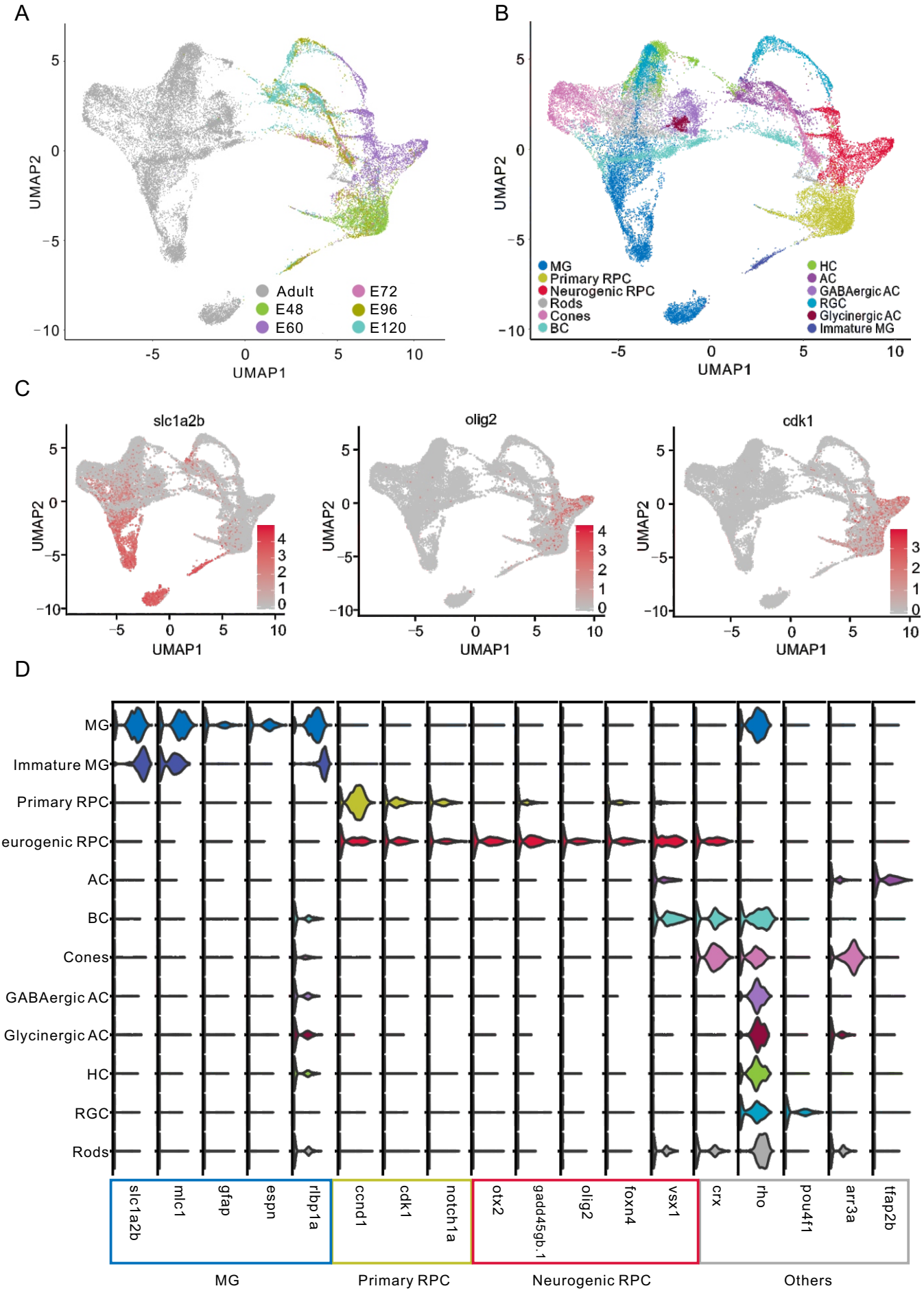

Figure S12, Hoang et al. Clustering of developing MG cells from zebrafish. (A) UMAP view of retinal samples from zebrafish development. (B) Clustering of retinal cells during zebrafish development. (C) Single-cell expression of marker genes in the development of zebrafish MG/RPCs. (D) Violin plot of known marker gene expression over the course of development of zebrafish MG/RPCs.

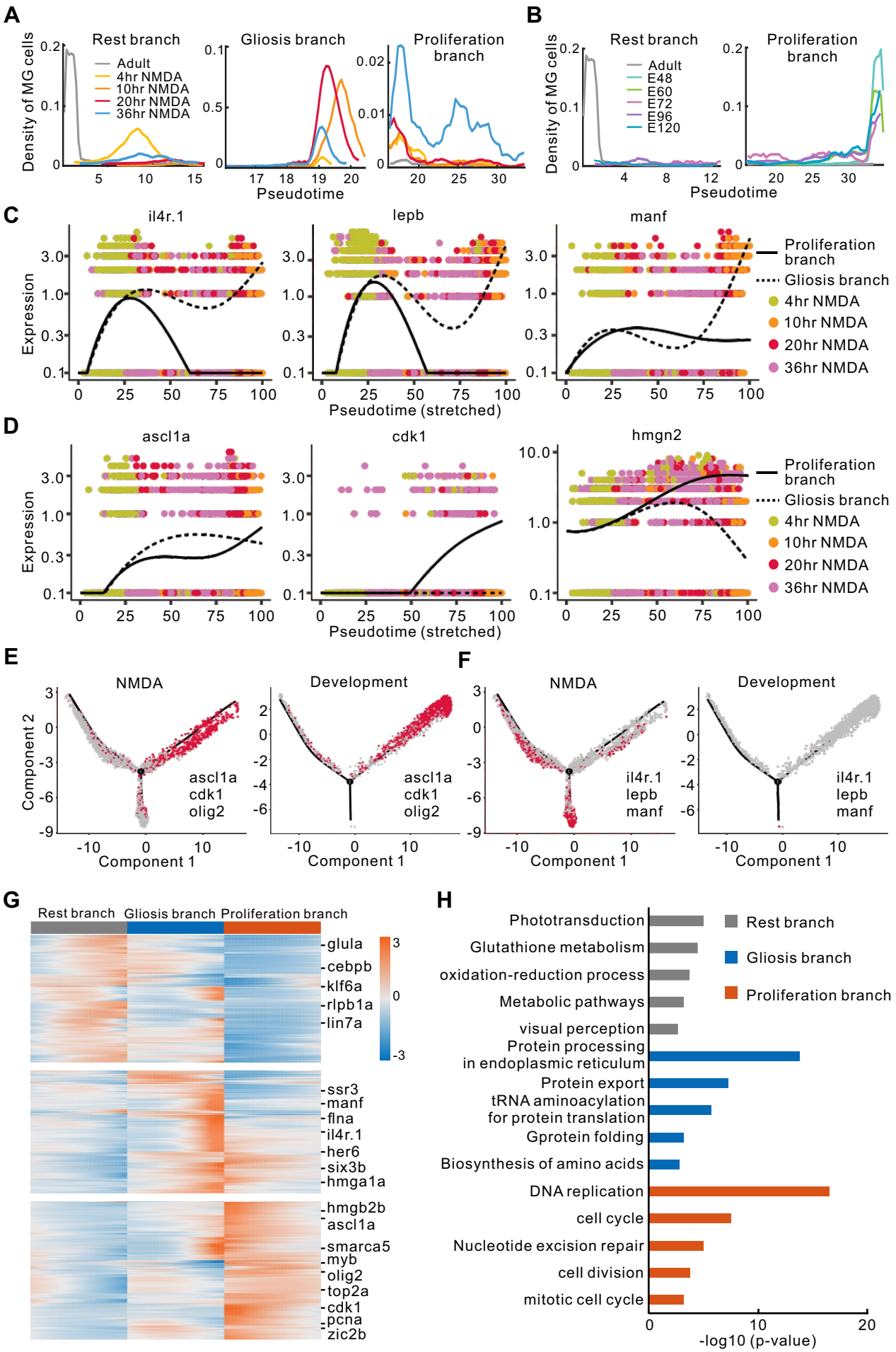

Figure S13, Hoang et al. Analysis of branch-specific expressed genes in zebrafish MG following NMDA treatment. (A) The density of zebrafish NMDA-treated MG across pseudotime. (B) The density of zebrafish development cells across pseudotime. (C) Pseudo-temporal expression of genes enriched in the gliosis branch. (D) Pseudo-temporal expression of genes enriched in the proliferation branch. (E) Expression of neurogenic genes in zebrafish NMDA and development. AUC score was calculated to identify the cells expressing neurogenic genes. (F) Expression of gliotic genes in zebrafish NMDA and development. Red dots indicate actively expressed cells with high AUC score. (G) Heatmap of genes specifically expressed in each of the three branches. (H) Top functions of enriched genes in three branches.

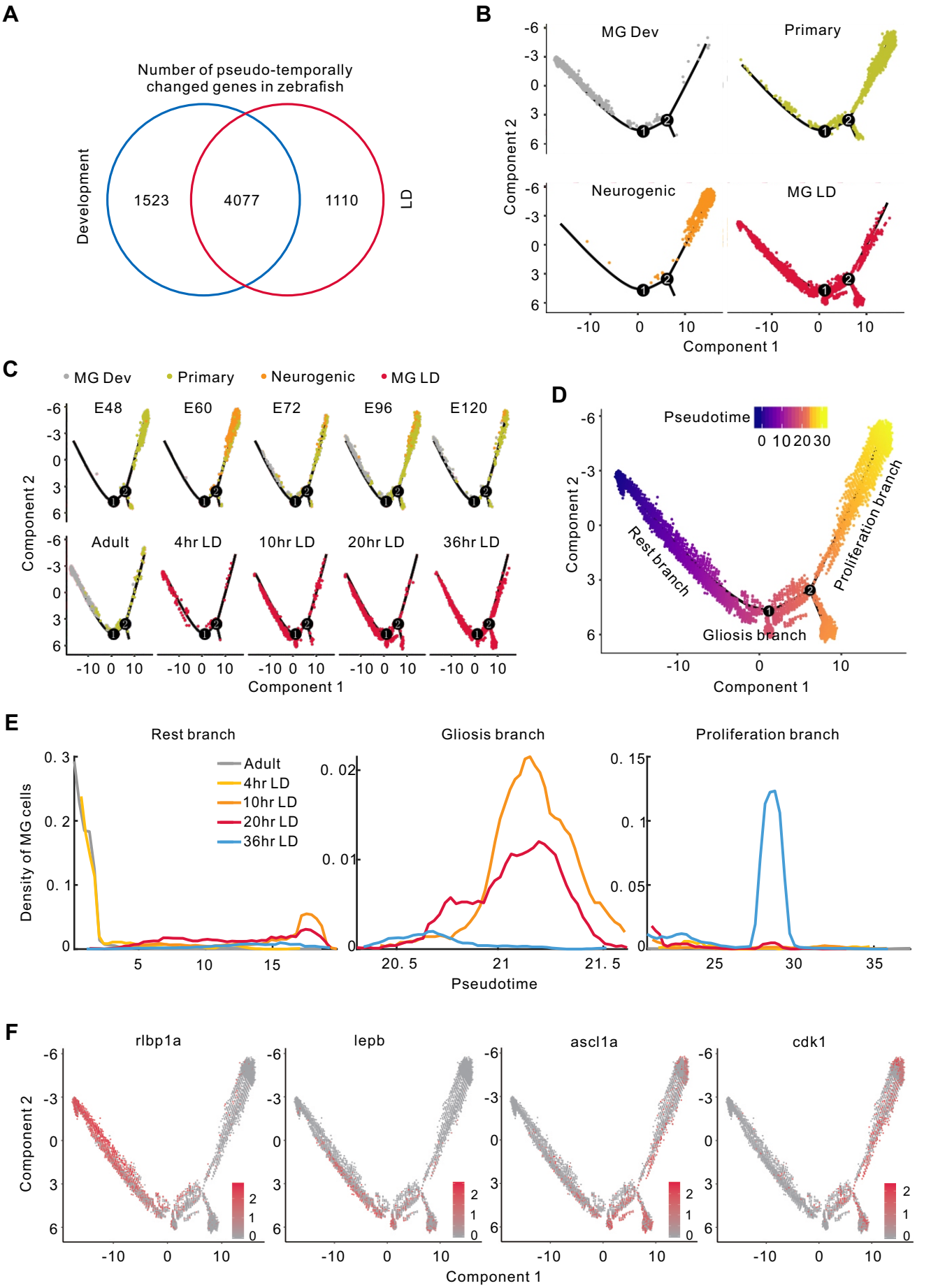

Figure S14, Hoang et al. MG trajectory analysis for zebrafish development and light damage. (A) Venn diagram of the number of pseudo-temporally changed genes in zebrafish development and light damage (LD). (B) MG/RPC trajectory from zebrafish development and light damage, separated by cell types. (C) MG trajectory from zebrafish development and light damage, separated by real time. (D) MG pseudotime analysis during zebrafish development and following light damage. (F) The density of MG across pseudotime of zebrafish light damage. (E) Single-cell expression of rest/gliosis/proliferation-related genes in light damage samples.

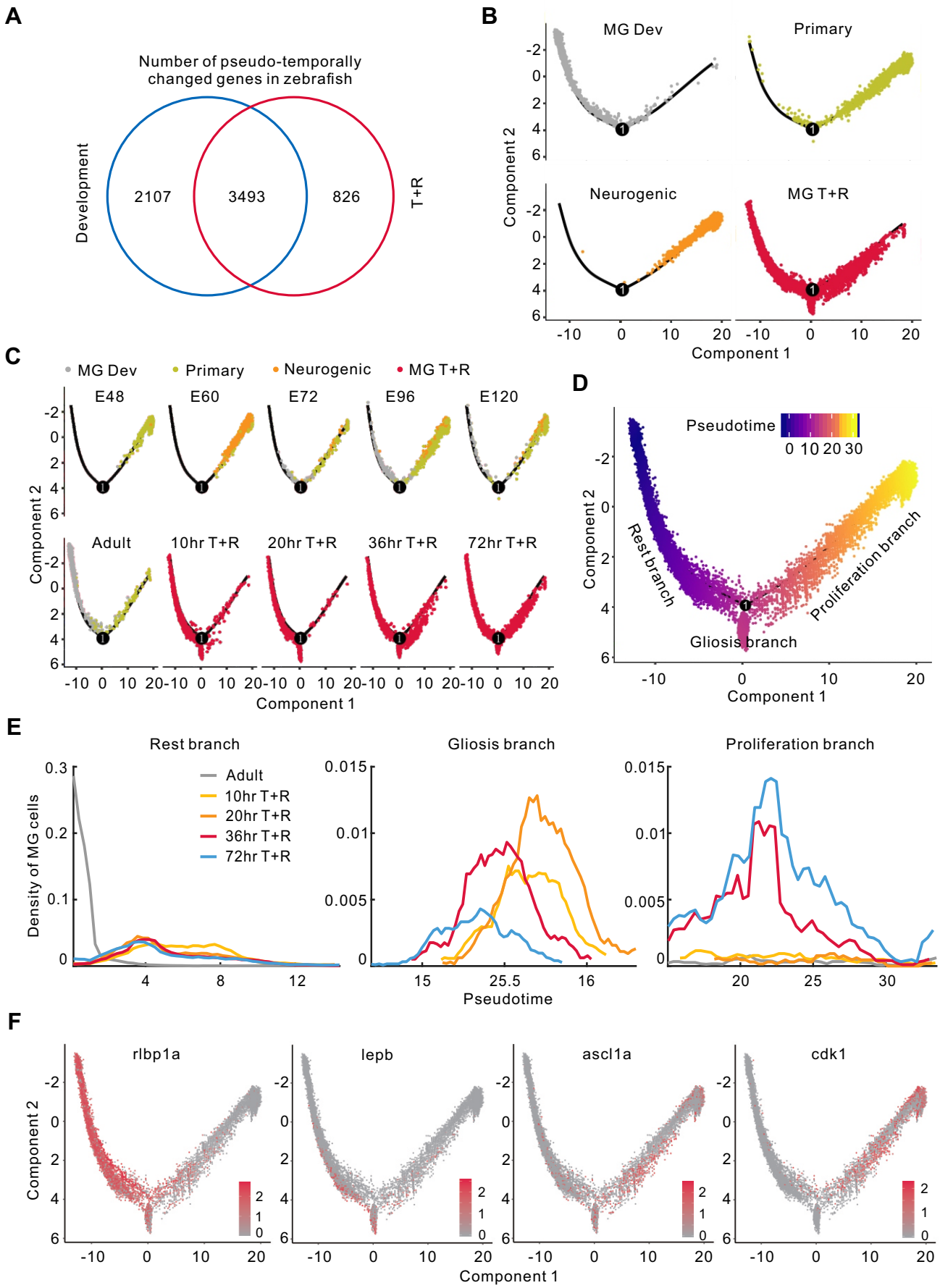

Figure S15, Hoang et al. MG trajectory analysis for zebrafish development and TNFa+RO4929097 (T+R) treatment. (A) Venn diagram of the number of pseudo-temporally changed genes from zebrafish development and T+R treated MG. (B) MG trajectory from zebrafish development and T+R treatment, separated by cell types. (C) MG trajectory of zebrafish development and T+R treatment, separated by real time. (D) MG trajectory and pseudotime of zebrafish development and T+R treatment. (F) The density of MG across pseudotime of zebrafish T+R treatment. (E) Expression of rest/gliosis/ proliferation-related genes following T+R treatment.

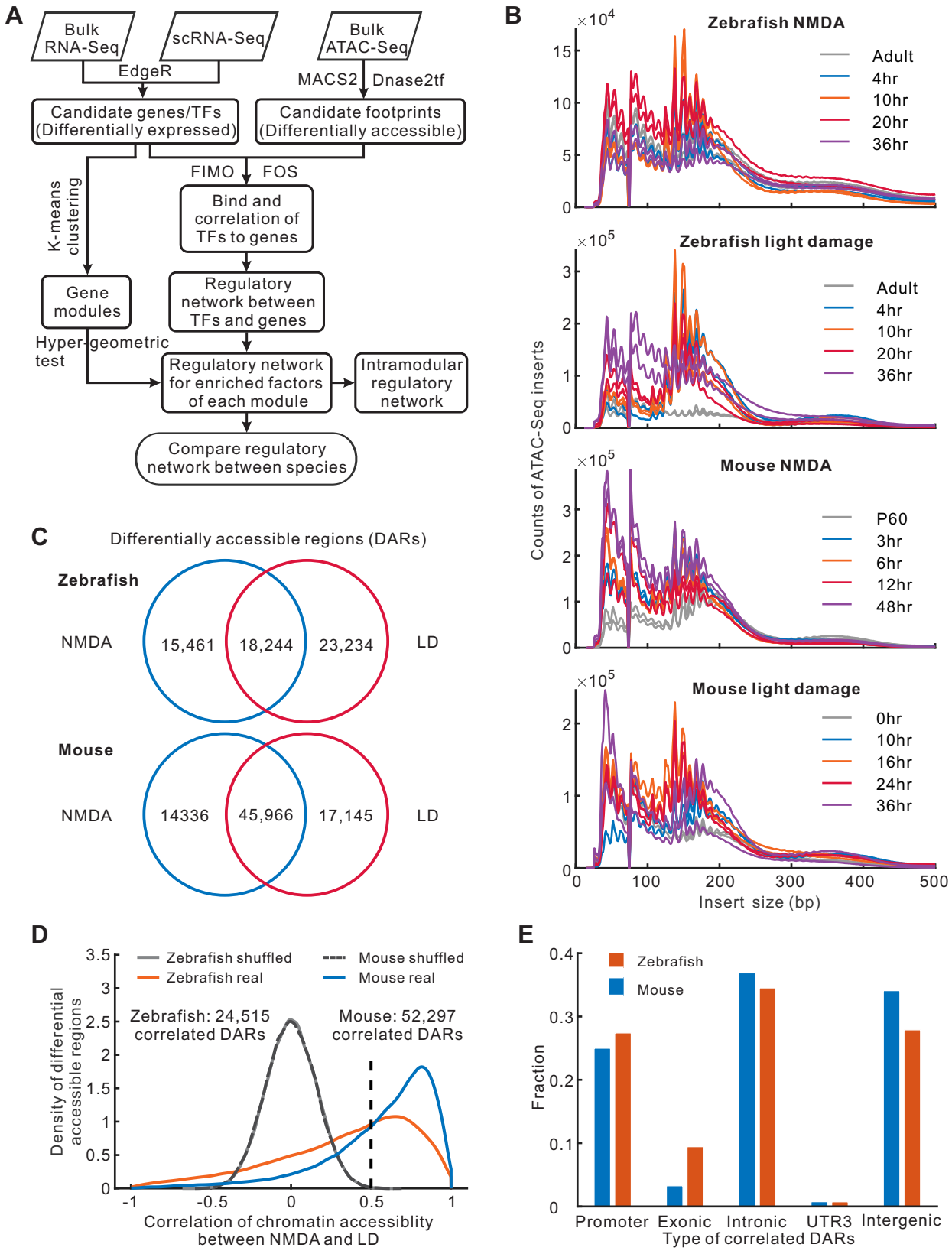

Figure S16, Hoang et al. Identification of differentially accessible regions (DARs) from ATAC-Seq data. (A) Workflow of Integrated Regulatory Network Analysis (IReNA) in integrating gene expression and chromatin accessibility to reconstruct regulatory network (see Methods). (B) Distribution of ATAC-Seq inserts. (C) Number of DARs in NMDA treatment and light damage (LD) of zebrafish and mouse. (D) Distribution of DAR correlations between two models. (E) Fraction of five types of correlated DARs.

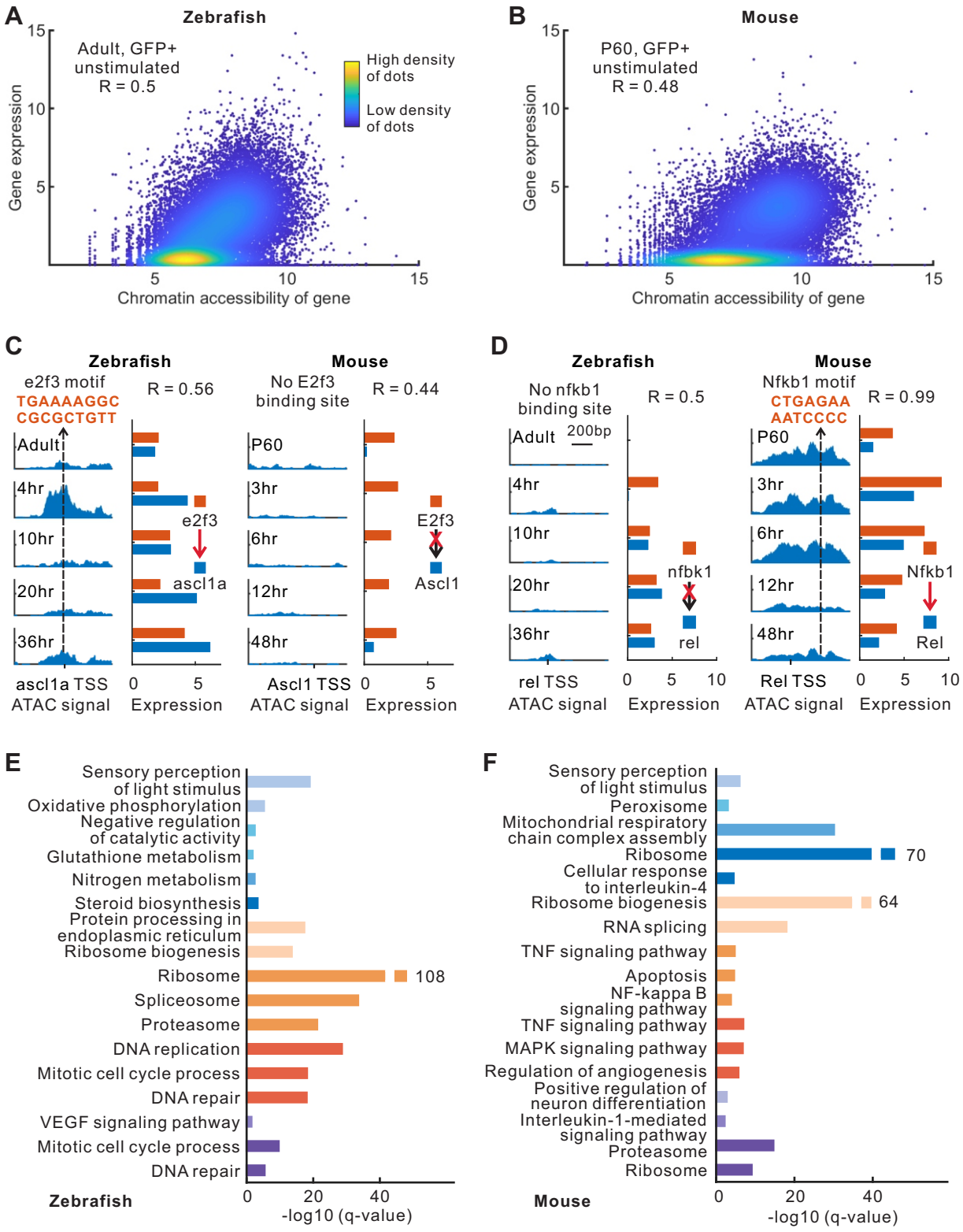

Figure S17, Hoang et al. Changes in chromatin accessibility and gene expression. (A-B) Correlation of gene expression and corresponding chromatin accessibility in zebrafish and mouse. Each dot represents one gene. (C-D) Changes in chromatin accessibility and expression for two regulatory gene pairs of e2f3/ascl1a in zebrafish and Nfkb1/Rel in mouse. TSS, transcription start site. (E-F) Most highly enriched functions of each gene module in zebrafish and mouse. Colors represent gene modules.

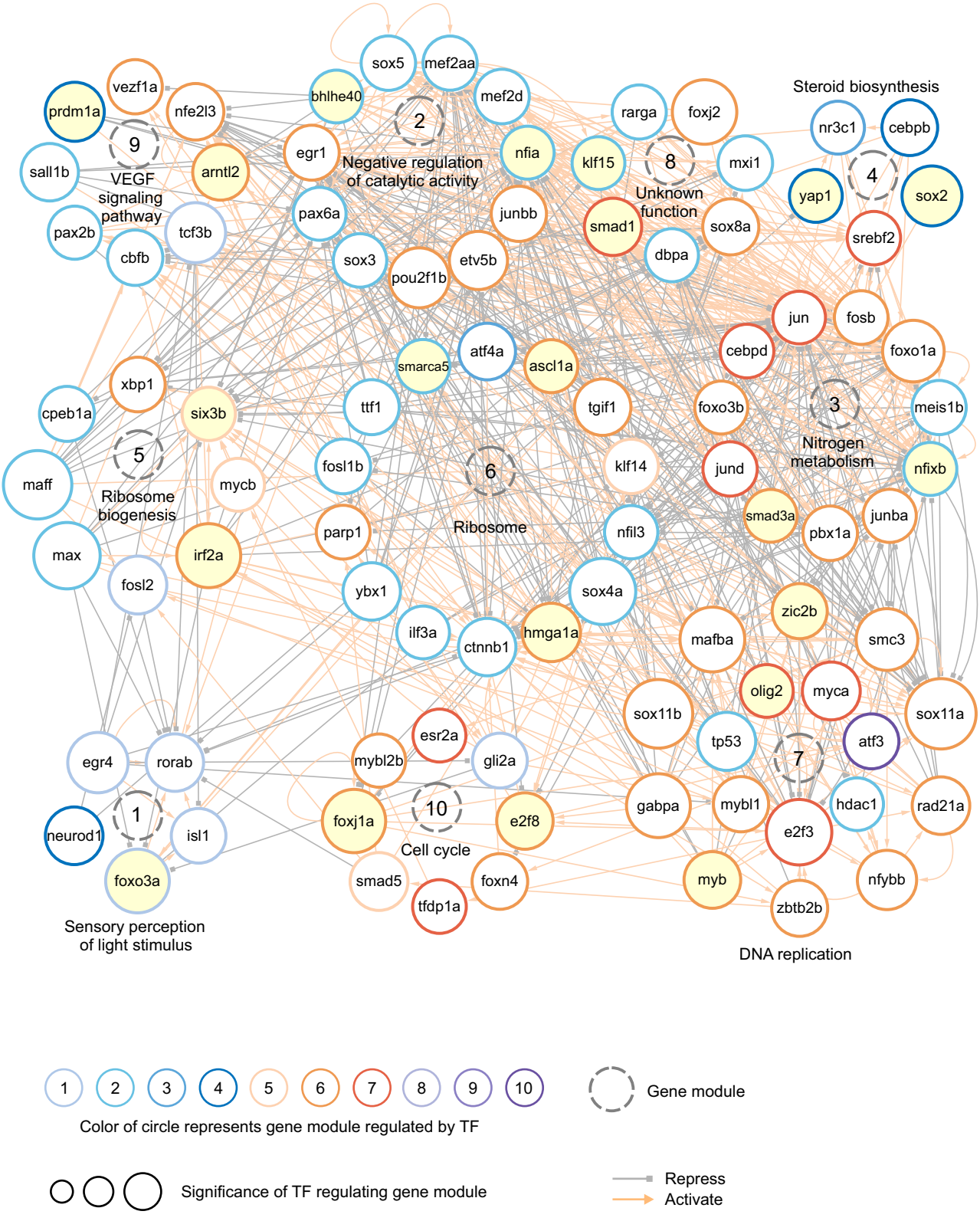

Figure S18, Hoang et al. Regulatory network of enriched TFs in the zebrafish. Enriched TFs are separated into ten modules based on TF expression pattern from Figure 6B. For each enriched TF, the most significantly regulated module was used to label the color of the circle. Circles filled in yellow indicate key regulators.

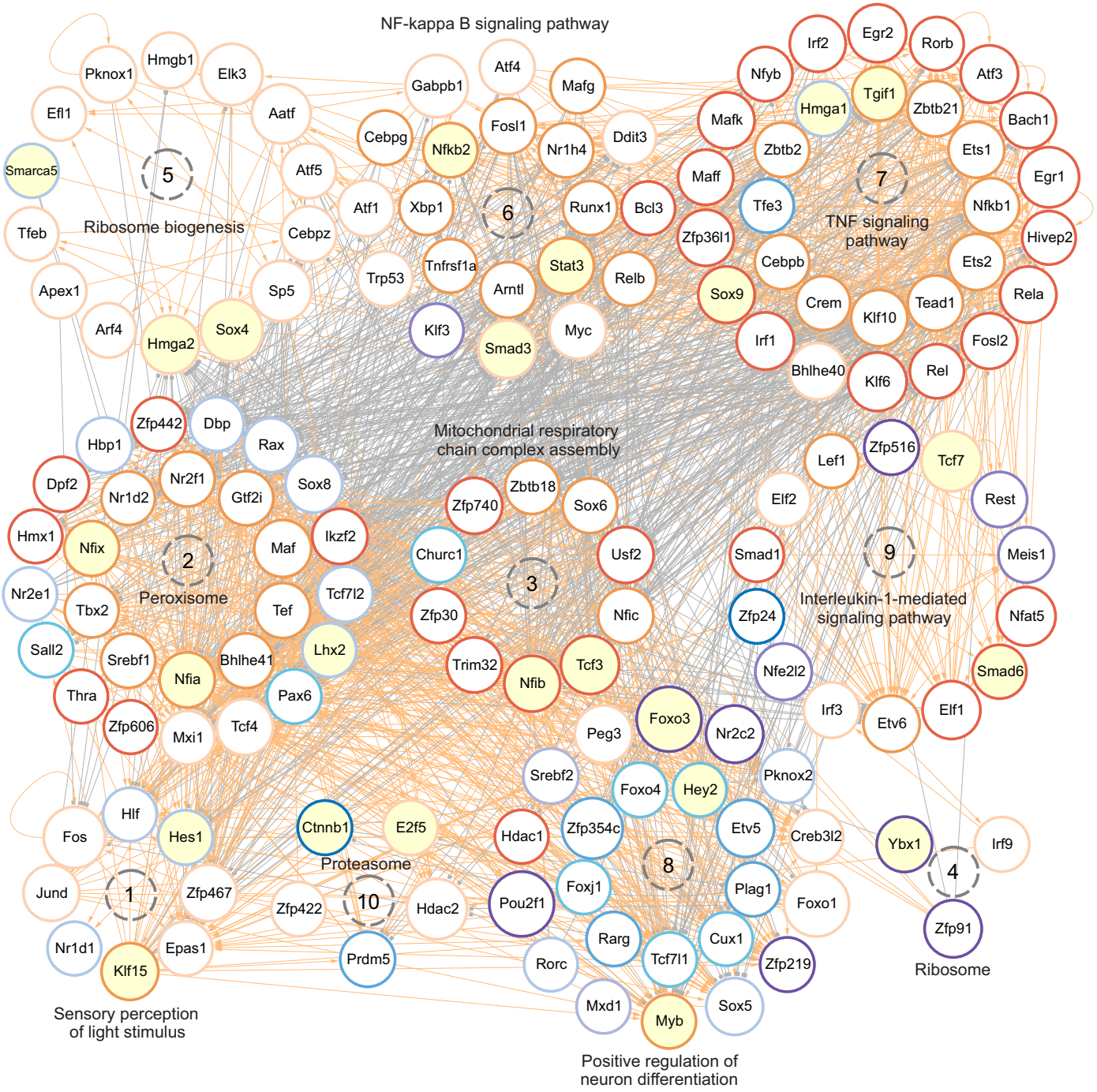

Figure S19, Hoang et al. Regulatory network of enriched TFs in the mouse. Enriched TFs are separated into ten modules based on TF expression pattern from Figure 6C. For each enriched TF, the most significantly regulated module was used to label the color of the circle. Circles filled in yellow indicate key regulators.

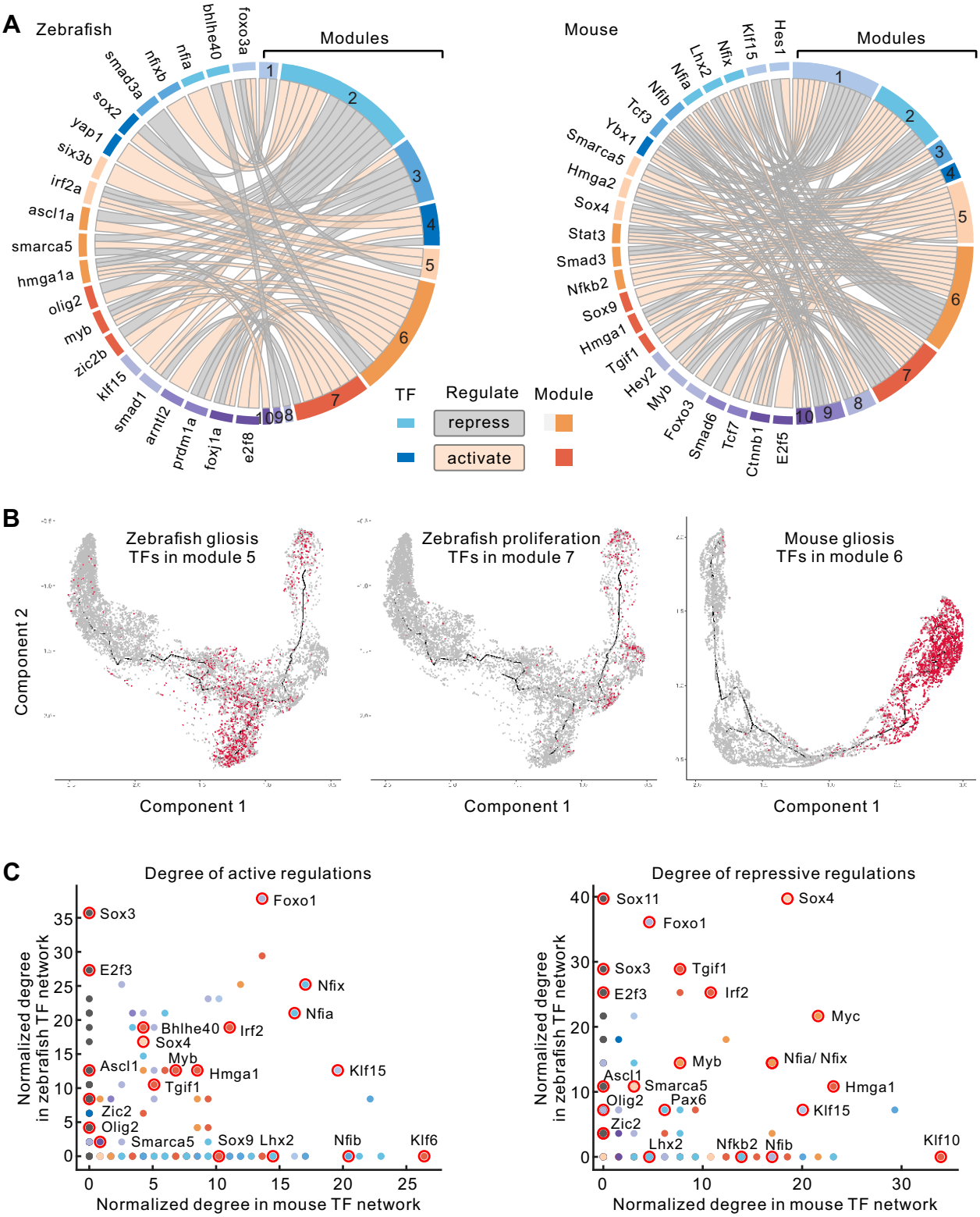

Figure S20, Hoang et al. Features of enriched TFs. (A) Significant regulations between TFs and modules in zebrafish and mouse. Color of individual TFs match their associated modules. (B) Single-cell expression of TFs from gliosis/proliferation-related modules in zebrafish and mouse. Red dots indicate cells actively expressing gliosis/proliferation-related TFs. (C) Comparison of the regulation degree of enriched TFs between mouse and zebrafish. Color of dots represents the module of TFs in the mouse. Black dots indicates that the TF is not enriched in TF networks observed in the mouse. Dozens of key TFs are highlighted in red circles.

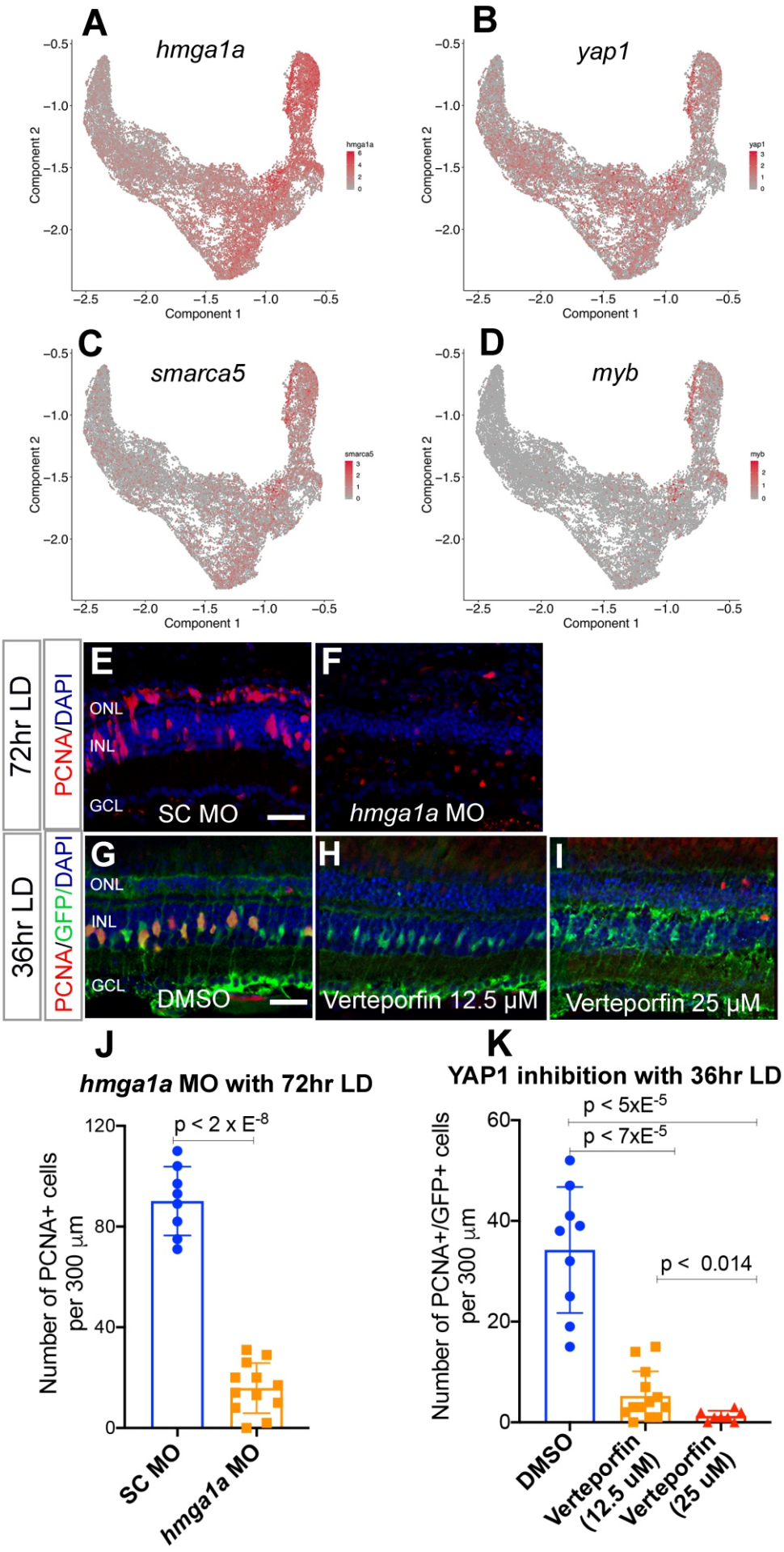

Figure S21, Hoang et al. Candidate genes that regulate zebrafish MGPC formation in the damaged retina. (A-D) Expression of candidate genes in zebrafish MG trajectory from NMDA, light damage and TNFa+RO4929097 (T+R) treatment. (E-F) PCNA expression in standard control and hmga1a morphant retinas after 72 hours of light treatment. (G-I) PCNA and EGFP expression in DMSO control and Verteporfin-treated albino; Tg[gfap:EGFP]nt11 retinas after 36 hours of constant light. (J) Quantification of the number of PCNA-positive INL cells in standard control, and hmga1a morphant retinas at 72 hours of constant light. (K) Quantification of the number of PCNA and EGFP colabeled INL cells in DMSO control and Verteporfin-treated retinas at 36 hours of constant light. Scale bars in panels E and F represent 20 µm.

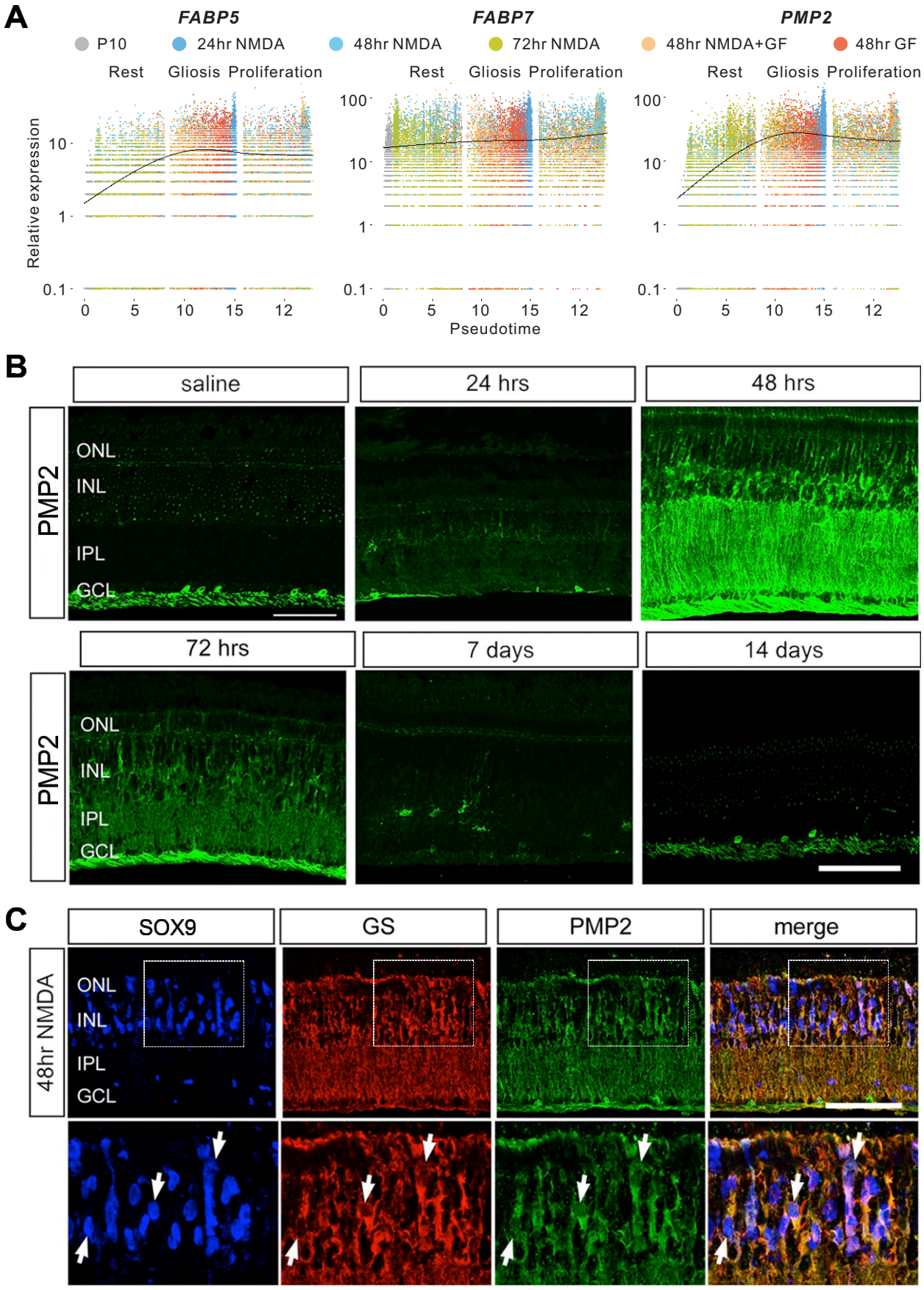

Figure S22, Hoang et al. Expression of FABP5, FABP7 and PMP2 (FABP8) was induced in chick MG after NMDA injury. (A) Pseudo-temporal expression of FABP5, FABP7 and PMP2 in the chick MG during NMDA damage. (B) Immunohistochemistry shows a transient upregulation of expression of PMP2 protein at 48 and 72 hr after NMDA-induced injury in chick retina. (C) Increased expression of PMP2 in the MG as indicated by co-localization of PMP2 with SOX9 and GS proteins (white arrows). Scale bar, 50 μm.

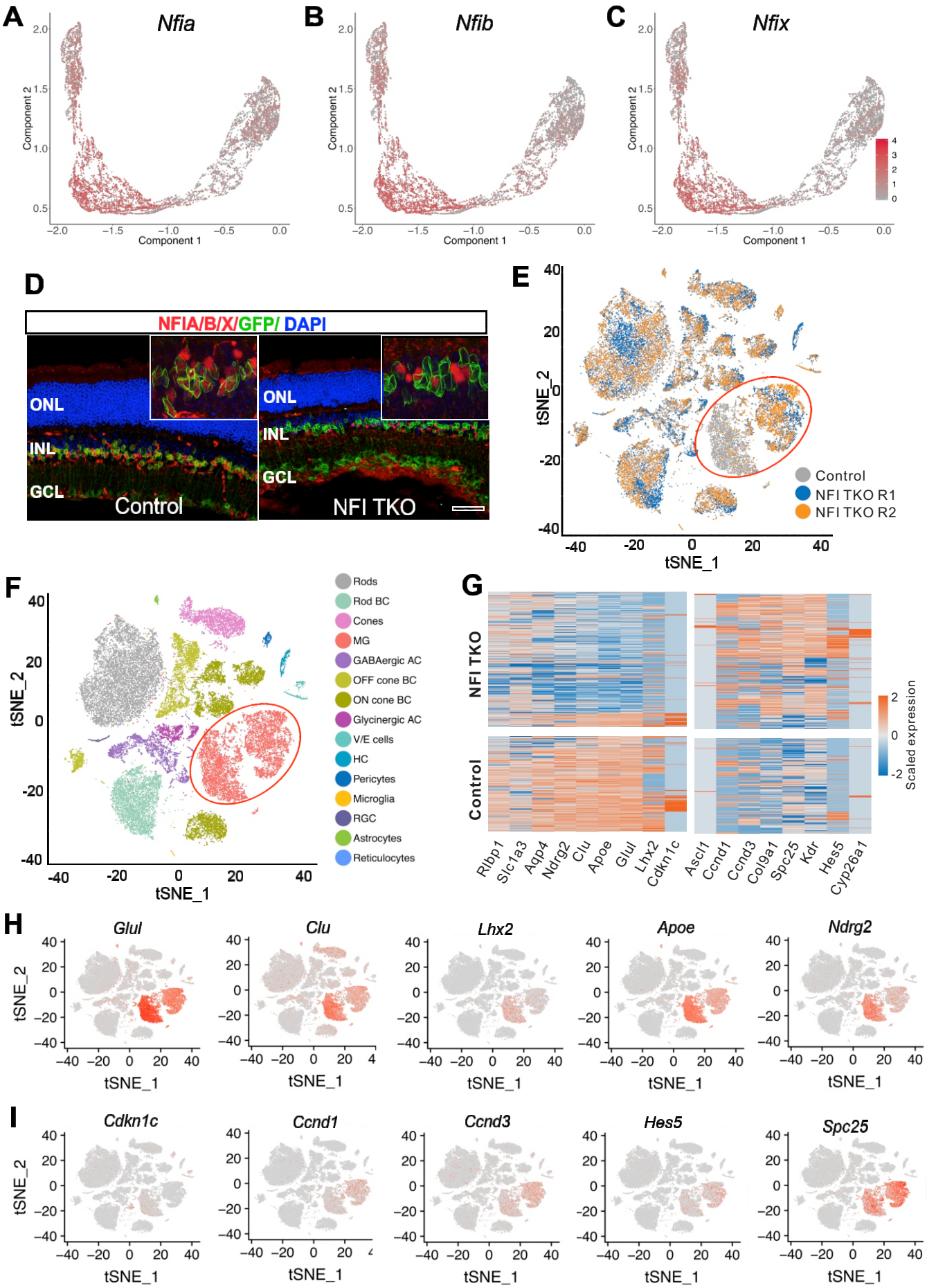

Figure S23, Hoang et al. Loss of Nfia/b/x led to downregulation of MG markers and upregulation of cell cycle-related genes in mouse retina. (A-C) Expression of Nfia/b/x in mouse MG during NMDA injury. (D) Immunohistochemistry indicates a MG-specific deletion of Nfia/b/x in adult NFI TKO mouse retina as compared with the control. (E) tSNE view of single cells from the aggregation of two NFI TKO retinal samples and a control retinal sample. (F) tSNE view of cell types from the aggregation of two NFI TKO and a control retinal samples. MGs from NFI TKO samples are clearly distinct from the control sample. (G) Single-cell heatmap shows a set of DEGs of the MG from the two mouse genotypes. (H) tSNE view shows a down-regulation of the MG markers in the NFI TKO retinas. (I) tSNE view shows genes that were up-regulated in the MG in the NFI TKO retinas as compared with control.